Sun et al. EURASIP Journal on Wireless Communications and Networking (2019) 2019:145
https://doi.org/10.1186/s13638-019-1465-6

EURASIP Journal on Wireless Communications and Networking

RESEARCH Open Access

Study on reflectivity data interpolation and mosaics for multiple Doppler weather radars

Min Sun[1], Haijiang Wang[1*], Zhaoming Li[2], Mengqing Gao[1], Zili Xu[3] and Jing Li[3]

Abstract

Multiple weather radars' joint detection can enlarge the radar detection range and can improve the detection accuracy, which has become an important method to monitor large-scale weather effectively. In this paper, the methods of interpolating reflectivity volume scan data onto the grids in the Cartesian coordinate system and three-dimensional mosaic for gridded reflectivity data of several radars are studied. In order to retain the physical characteristics of the raw data, the smoothing parameters of adaptive Barnes interpolation are improved which based on the space structure of the raw reflectivity data. Through comparison of constant altitude plan position indication (CAPPI) images obtained by the commonly used interpolation schemes and the improved Adaptive Barnes interpolation, it was found that the latter can provide consecutive reflectivity fields and retain high-resolution structure comparable to the raw data. The mean deviation filter filtering erroneous grid data and the data are fused by various fusion methods. Result shows that Exponential Weighting is an excellent method which can provide continuous three-dimensional reflectivity mosaic data.

Keywords: Smoothing parameters, Adaptive Barnes interpolation, CAPPI, Mosaics

1 Introduction

Doppler weather radar is the primary sensor for observing precipitation with high temporal and spatial resolution, which is highly advantageous in mesoscale meteorological research [1]. The coverage of the single immobile Doppler radar is too limited to detect large-scale weather systems, such as Meiyu, squall lines, and so on. Such a limitation obstructed us from further revealing the laws of the atmospheric movement relevant to those weather systems. Joint detection of multiple Doppler radars can provide a wider range and higher quality.

The National Severe Storms Laboratory utilized the infrastructure to integrate the radars within a system to produce a 3D radar mosaic grid for the USA [2]. Zhang et al. developed a national 3D radar reflectivity mosaic system [3] which was applied to assimilating data for convective scale numerical weather modeling and other uses. National Severe Storms Laboratory has developed a four-dimensional dynamic grid (4DDG) to accurately represent discontinuous radar reflectivity data over a continuous 4D domain [4]. Mark A et al. applied the Adaptive Barnes algorithm to radar data interpolation [5]. Lakshmanan V et al. described a technique for taking the reflectivity data, and derived products from multiple radars and combining them in real time into a rapidly updating 3D merged grid [6]. Because the vertical distribution of precipitation echoes is inhomogeneous [7], it is essential to interpolate data into the same height to reflect the precipitation intensity better. The common interpolation methods include the Nearest Neighbor [8], Vertical Horizontal Linear interpolation [9, 10], the Cressman Weighting scheme [11], and Barnes interpolation [12, 13]. Trapp et al. [14] studied the smoothing and filtering characteristics of these simple analytical methods through theoretical consideration. Huang et al. [15] tested the effects of these mainly used interpolation and mosaic methods. Although the Cressman has been widely used for spatial objective analysis of radar data, the Barnes filter may be preferable owing

* Correspondence: whj@cuit.edu.cn
[1]College of Electronic Engineering, Chengdu University of Information Technology, Chengdu 610225, Sichuan, China
Full list of author information is available at the end of the article

to the ease of computation of the response function of the Barnes filter [16]. Zhang considered that the spatial interpolation technique should be minimally smooth in radar data and retains the original echo structure features apparently in the single radar data as much as possible [3].

Radar data gridding and mosaic is of great significance in meteorological service [17]. The mosaics of the basic reflectivity of multiple weather radars can expand the detection range, detect large-scale weather, and improve the accuracy in overlapping areas. Mosaics can also mitigate various problems caused by the geometry of radar beam such as void data with the cone of silence above the radar and in regions below the lowest beam [18]. The common radar mosaics methods include the Maximum Value method, Nearest Neighbor method, Inverse Distance Weight method, and Arithmetic Average method. Moreover, Li has designed and developed an echo mosaic platform based on the systematic study of radar mosaic algorithms, techniques, and software programs [19]. There are two fundamental characteristics with radar data. One is that the distribution of radar data depends on the direction, and the other is that the radar data density distribution decreases as the distance increases. In space, with the increase of elevation and slope distance, the spatial resolution of radar reflectivity data becomes larger [20, 21].

The three-dimensional mosaic technology of the Next Generation Weather Radar (NEXRAD) includes three aspects in this paper, data processing, interpolation of single station, and mosaic of multiple radars. The former involves gridding reflectivity data, and calculating the common coverage areas of three radars as Section 2. Then interpolation methods are introduced in Section 3. Finally, filtering scheme and the three-dimensional mosaic process are shown in Section 4. In Section 5, reflectivity mosaics of the three radars in Sichuan province of China are obtained based on the Adaptive Barnes interpolation method and Exponential Weighting method.

2 Data

The distribution of multiple radars and the consistency of data time are two basic conditions of joint detection. Studies have shown that the closer three radars' position are to the equilateral triangle, the better the fusion effect [22, 23]. Go without saying, the time difference of radars data should be as small as possible to ensure simultaneity.

In this research, a large amount of precipitation data from three CINRAD-SC weather radars in Sichuan province of China has been collected, and the parameters are showed in Tables 1 and 2. Precipitation scan data at the same time (interval less than 5 min) from July 2 to July 7 reflect the detailed precipitation process. The echo data of three radars of the same model is relatively uniform.

Table 1 The location of three radars

Radar number	Location	Latitude	Longitude
Z9280	Chengdu, Sichuan	30.6600	104.01
Z9816	Mianyang, Sichuan	31.4522	104.765
Z9817	Nanchong, Sichuan	30.8219	106.0778

Combined with the parameters of these radars, the detective coverage can be obtained as shown in Fig. 1.

Radar beams is conically scanning at each elevation angle when volume scanning. Therefore, the radar echo data is stored in the form of a polar coordinate system (elevation, azimuth, and slope distance) in which the pole is radar station. The spatial resolution increases with the raise of elevation and slope distance. It is imperative to unify the scattered data onto a spatial grid with uniform resolution. Symmetrical grid is set both in the horizontal and vertical directions, and the horizontal resolution is 200 m × 200 m and vertical interval is 1 km (2 km~ 6 km, five layers).

Basic reflectivity data are interpolated on the grid points in spherical coordinates, and then it is converted into Cartesian coordinates (longitude, latitude, height) to mosaic and display. The arc length between the vertical projection point of a grid point at any height to the surface of the earth and the radar station is L, then

$$L = R \times \sin^{-1}\frac{r}{R+h} \approx r \tag{1}$$

$$\phi = \phi_0 + y/D_\phi \tag{2}$$

$$\lambda = \lambda_0 + x/D_\lambda \tag{3}$$

Where R is the radius of the earth, and h, ϕ, λ are the height, latitude, and longitude of the grid point, and r is the distance between grid point to radar station, and D_ϕ, D_λ are arc length spanning unit latitude and longitude, and x, y are horizontal and vertical distances between

Table 2 The main technical indicators of CINRAD-SC weather radar

Number	Project	Radar (CINRAD-SC)
1	Transmitter WAVE type	C-band (5630 Mhz)
2	Transmitter Peak power	660 Kw
3	Antenna type	4.5 db
4	Beam width	0.9°
5	Detection range	160 km
6	Range Bin	300 m
7	Volume scan mode	VCP21
8	Elevation range	0.5–19.5
9	Scan mode	PPI

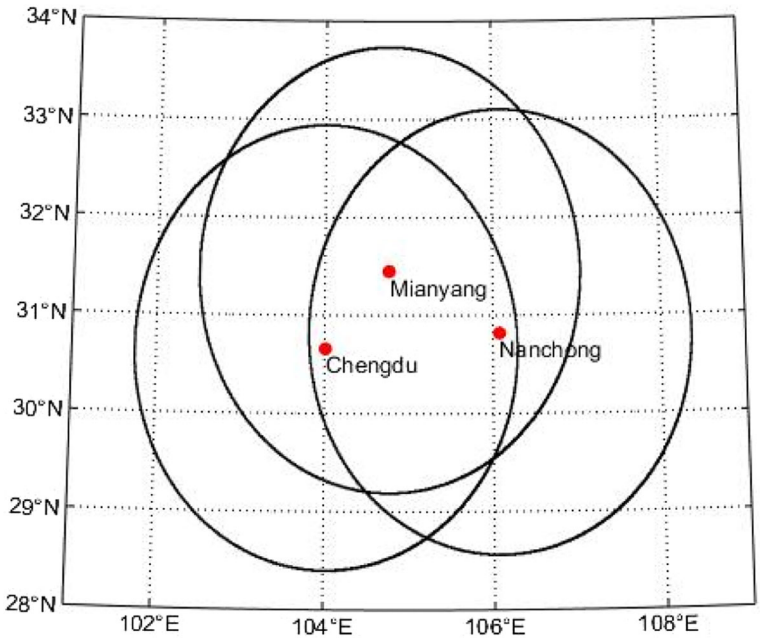

Fig. 1 The detective coverage of three Doppler weather radars

grid points and radar stations, and ϕ_0, λ_0 are the latitude and longitude of radar station.

3 Interpolation algorithm

The data obtained by radar scans at a certain elevation are not in the same plane coordinate system, but in the spherical coordinate. In this paper, several common interpolation methods are introduced and compared, including the Nearest Neighbor method, Vertical Horizontal Linear interpolation method, 8-point Linear interpolation method, and Adaptive Barnes interpolation method.

3.1 Nearest Neighbor

In 3D space, the nearest range bin is used to fill the grid cell. This method depends on the distance between the grid cell and range bin center. The nearest rang bin is unique object of reference. This method produces instable and discontinuous data possibly. Although the Nearest Neighbor method is the simplest method, it is not an advisable choice to use it in most case.

3.2 Vertical Horizontal Linear interpolation

The schematic of Vertical Horizontal Linear interpolation (VHI) is showed in Fig. 2, where (r, a, e) is polar coordinates of grid points, and r, a are slope distance, azimuth. Moreover, e is elevation located between adjacent elevation e_1 and e_2. L_1, L_2 are the intersecting lines of adjacent elevation layers and vertical plane which pass through poles and (r, a, e). The Nearest Neighbor method is adopted in radial and azimuth. (r, a, e_1), (r, a, e_2) are intersection of the vertical line passing through grid point and the axis of the adjacent elevation beam. (r_1, a, e_2), (r_2, a, e_1) are intersection of the horizontal line passing through grid point and the axis of the adjacent elevation beam. r_1 and r_2 can be determined by Eq. (4).

$$\begin{cases} r_1 = r \ \sin e / \ \sin e_2 \\ r_2 = r \ \sin e / \ \sin e_1 \end{cases} \tag{4}$$

Then the grid can be determined by VHI:

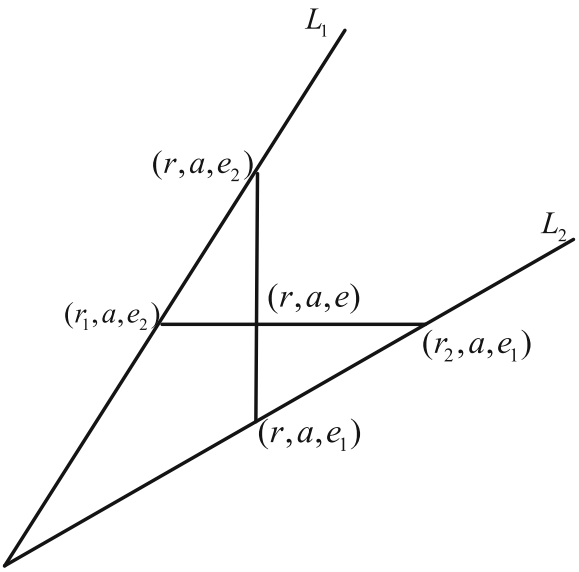

Fig. 2 The detective coverage of three Doppler weather radars

$$Z(r,a,e)=\frac{(w_{e1}Z(r,a,e_1)+w_{e2}Z(r,a,e_2)+w_{r1}Z(r_1,a,e_2)+w_{r2}Z(r_2,a,e_1))}{w_{e1}+w_{e2}+w_{r1}+w_{r2}} \tag{5}$$

Among the expression, w_{e1}, w_{e2}, w_{r1}, w_{r2} are the weights of $Z(r,a,e_1)$, $Z(r,a,e_2)$, $Z(r_1,a,e_2)$, and $Z(r_2,a,e_1)$ which can be obtained by Eqs. 6 and 7.

$$\begin{cases} w_{e1}=(e_2-e)/(e_2-e_1) \\ w_{e2}=(e-e_1)/(e_2-e_1) \end{cases} \tag{6}$$

$$\begin{cases} w_{r1}=(r_2-r)/(r_2-r_1) \\ w_{r2}=(r-r_1)/(r_2-r_1) \end{cases} \tag{7}$$

3.3 8-point Linear interpolation

Grid cell $f_0(r_0,a_0,e_0)$ falls into a quadrangular prism whose eight vertices are f_1~f_8. The grid cell can be obtained by Eq. (8).

$$\begin{aligned} f_0 = {} & w_{e1}[(w_{r1}f_1+w_{r2}f_2)w_{a1}+(w_{r1}f_3+w_{r2}f_4)w_{a2}] \\ & +w_{e2}[(w_{r1}f_5+w_{r2}f_6)w_{a1}+(w_{r1}f_7+w_{r2}f_8)w_{a2}] \end{aligned} \tag{8}$$

Then, the interpolation weights in azimuth direction are:

$$\begin{cases} w_{a1}=(a_2-a)/(a_2-a_1) \\ w_{a2}=(a-a_1)/(a_2-a_1) \end{cases} \tag{9}$$

3.4 Adaptive Barnes

Barnes interpolation method is wildly used to project data with uneven resolution into the coordinate system of a grid with uniform resolution, and it is divided into uniform Barnes interpolation and the Adaptive Barnes interpolation. The difference is that the former is suitable for the equidistant Cartesian coordinate system, and the latter is used in the spherical coordinate system (Fig. 3). The Adaptive Barnes scheme is often applied to spatial objective analysis with the features of automatic adaptation to data density and direction splitting, and it is given by Eq. (10).

$$f_0=\frac{\sum_{k=1}^{N}w_k f_k}{\sum_{k=1}^{N}w_k} \tag{10}$$

Where, f_k is the value of a grid point from different radars, and the weight function is expressed as Eq. (11). Motivated by spatial characteristics of radar data and by the suggestions from Doswell [24], the weight function is split into three directions: radial, azimuthal, and elevational as shown in Fig. 4.

$$w_k=\begin{cases} \exp\left[-\frac{(R_k-R_0)^2}{k_r}-\frac{(\theta_k-\theta_0)^2}{k_\theta}-\frac{(\phi_k-\phi_0)^2}{k_\phi}\right] & \text{(where } f_k \text{ is valid)} \\ 0 & \text{(where } f_k \text{ is invalid)} \end{cases} \tag{11}$$

In the expression, R_k, ϕ_k, θ_k are the polar coordinate parameters of f_k, and k_r, k_ϕ, k_θ are smoothing parameters for slope distance, azimuth, and elevation which can be adjusted to achieve different smoothing effects.

The design of the Adaptive Barnes weight function allows the use of different smoothing parameters in different directions to accomplish direction splitting technique and it is better to adapt the anisotropy of the radar data spacing. There are two strategies to determine the Barnes smoothing parameters. The first general strategy is to fix the value of three smoothing parameters. This technique is a direction-splitting technique as mentioned above and it can produce weight function that is consistent with the dependence of radar data spacing on direction. And the smoothing parameters are selected according to the data density in the direction of the minimum density, which may cause the information collected in other directions to be interpreted as excessive smoothing. In the second strategy, labeled the matched filter (MF) strategy, the smoothing of equal-wavelength, one-dimensional waves in the radial, azimuthal, and elevation directions are matched, resulting in an isotropic filter. The smoothing parameters are

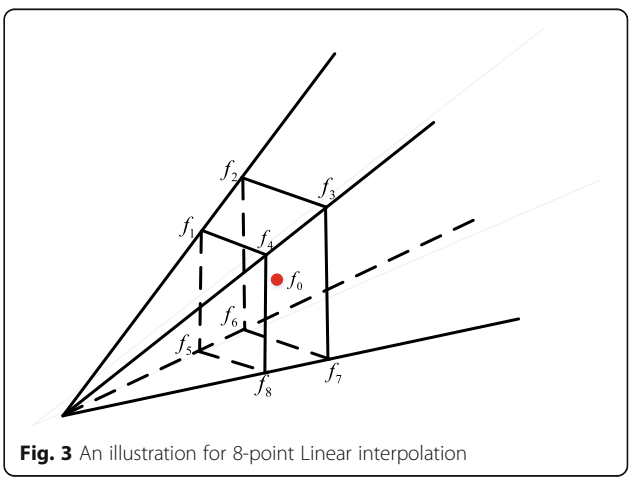

Fig. 3 An illustration for 8-point Linear interpolation

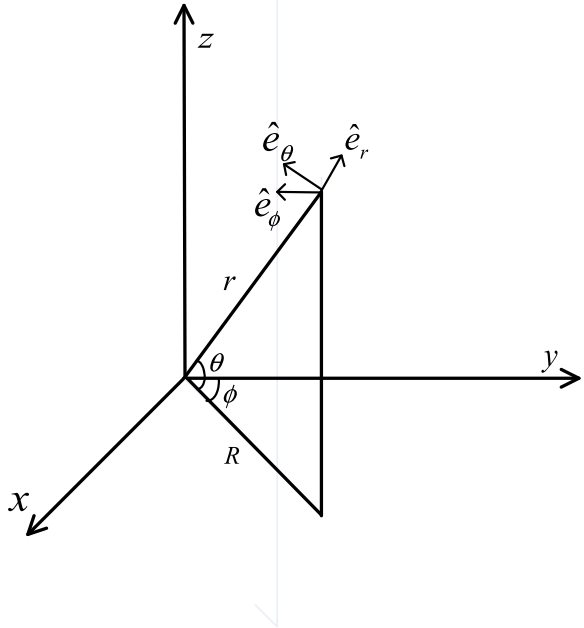

Fig. 4 The coordinate system for a fixed, ground-based weather radar. Where r is the radial distance, R is the distance between projection points of z plane and radar station, θ is elevation, φ is azimuth, and $\hat{e}_\varphi$, $\hat{e}_\theta$, $\hat{e}_r$ are vectors in the direction of azimuth, elevation, and radial

set according to the data coordinates and they vary with the coordinates of the analysis points, and that will result in the shape of the weight function and the filtering characteristics are not ascertainable. The shape of the weighting function is important for retaining the spatial reflectivity gradients and intensities. Different smoothing parameters are matched in different directions.

In the second scheme, the smoothing parameters are constructed based on the coordinates of the analysis points and the spatial structure of data, and they can be expressed by Eqs. (13) and (14).

$$k_r = R^2 \times k_\phi \tag{13}$$

$$k_\theta = \cos^2\theta \times k_\phi \tag{14}$$

k_r, k_ϕ, and k_θ are set, and the value of the other two parameters can be computed by Eqs. (13) and (14). The smoothing parameters are not fixed and they vary with the coordinates of the position of the sample point. In different situations, different fixed parameter is selected according to the data of spatial distribution characteristics and observer's goal. The spacing between sample points on the same radial is fixed (300 m). However, the data interval in azimuth direction increases with the increase of slope distance and elevation, and the data interval in elevation direction vary with the elevation spacing. If k_r is set and k_ϕ, k_θ are computed by using Eqs. (13) and (14), the Barnes weight function is fixed, isotropic, analogous to the first scheme which ignore two attributes of radar data. If k_ϕ is set and k_θ, k_r are computed by using the equations, the elevation and radial components will be filtered according to the resolution of the data in the azimuthal direction. The azimuth component is filtered equivalently at the same elevation angle and different distances. The high elevation angle is smoother at the same projection distance. Likewise, if k_θ is set and k_r, k_ϕ are computed, the azimuthal and radial components will be filtered according to the resolution of the data in the elevational direction. The elevation component is filtered equivalently at the same elevation angle and in different distances. At the same distance, the low elevation angle is smoother than the high elevation angle. In general, if the data interval in the elevation direction is much larger than the interval in the azimuth, it would be wise to set k_θ.

4 Mosaics

The keys of multiple weather radar mosaic are the accuracy and credibility of constant altitude plan position indication (CAPPI) data of each radar and mosaic algorithm. Therefore, it is indispensable to filter the reflectivity data involved in mosaics and to adopt a suitable mosaic algorithm.

4.1 Mean deviation filter

The quality of radar data depends on the performance of radar on transmitting and receiving, the precise calibration of radar system, and the effective quality control in the process of data acquisition and product generation. In the overlap areas of multiple radars, the grid data from three radars may be in great difference at the same grid points. One reason is that the characteristics of each radar are possibly diverse. The deviation is possibly caused by the difference in the distance from various radars. Other external factors and radar hardware problems might also have influence in the quality of radar data. The data of multiple radars at the same grid cell are stored in P sequence. The mean deviation of each data in the sequence can be calculated by Eq. (16).

$$dv_i = P_i - avP \tag{15}$$

$$avP = \sum_{i=1}^{N} \frac{P_i}{N} \tag{16}$$

Where, N represents the number of data in the same grid cell, P_i is the element in sequence P, avP is the mean value of sequence P, and dv_i is the mean deviation of elements. The threshold of mean deviation is set by M. If $dv_i > M$, it means that there is a problem with the

data and we need to delete it from the sequence. Otherwise, this data can be remained.

4.2 Reflectivity data mosaic

The CAPPI reflectivity data from multiple radars is efficiently fused to improve the accuracy of weather detection. The main methods include:

1. Nearest Neighbor

The nearest neighbor method assigns the value of grid cell which is closest to radar station to the grid cell. The results produced by this method are relatively rough, and the mosaic is seriously affected by the quality of radar data.

2. Maximum Value

The maximum value method includes comparing the analysis values of multiple radars in the same grid cell and assigning the maximum value to the grid cell. The advantage is that it is simple and easy to achieve, but it will cause errors in overlap areas.

3. Exponential Weighting method
   The method is based on the distance between the grid point and the radar station. There are many weight functions, in which the exponential weighting can construct nonlinear relationship between data which can be expressed as shown in the Eq. (17).

$$Z = \frac{\sum_{n=1}^{N} w_n \times Z_n}{\sum_{n=1}^{N} w_n} \tag{17}$$

Where N is the number of radars and w_n is weight parameter which can be showed as follows:

$$w_n = e^{-\frac{r_n^2}{R^2}} \tag{18}$$

Where r is the distance from the grid point to the radar station and R is equal to 100.

5 Result and discussion

5.1 Interpolation methods verification

CAPPI images at the height of 3 km as shown in Fig. 5 are obtained by adopting echo data detected by the Z9280 at 9:20 am on July 2, 2018 and by using the Adaptive Barnes interpolation algorithm and other commonly used methods (VHI, the Nearest Neighbor, 8-point Linear interpolation).

The value of a grid cell is determined by the linear relationship in elevation and azimuthal by VHI, and it is influenced by nearby vertical and horizontal data. From Fig. 5a, the data is smoothed linearly and excessively in the radial direction, causing the reflectivity CAPPI image to be distorted. Moreover, the intensity of reflectivity is weakened on the whole, especially in the heavy rainfall area. While the elevation is less than 20°, the two horizontal influential values have less influence on the grid cell. Hence, when the horizontal influential value is taken at a lower elevation, it may exceed the radial detection distance. The Nearest Neighbor method does not show any smoothing and linear processing on the data, therefore the mutation occurs in Fig. 5b. The Nearest Neighbor method is unstable and it is greatly affected by the interval and quality of original data. The 8-point Linear interpolation method is consistent with other methods in the size and intensity of heavy rainfall areas, and it has better total effects. However, there are many blank areas in the marker position.

The elevation range of CINRAD-SC radar scan from 0.5° to 19.5°, but the azimuth spacing on the same elevation layer is about 1°. The k_θ is fixed and k_r, k_ϕ are calculated by Eqs. (13) and (14). The matched filter strategy smooths grid data in different directions, making the CAPPI images smoother and have better anti-noise ability, and the intensity and extent of the heavy precipitation can be more precise. The eight adjacent grid cells determined by adjacent elevation, radial, and azimuth are regarded as the impact point. The smoothing parameters of the three directions are set according to the spatial structure, making the overall smoothness better without distortion.

The performance of the interpolation algorithm can be judged from the proportion of points with valid data, the smoothness and continuity of the generated image, and the location and heavy precipitation areas as shown in Table 3.

In the current experimental environment, it is a wise choice to fix k_θ and calculate k_r, k_ϕ. We should choose to fix one of the three according to the actual situation and the structure of data.

5.2 Mosaics verification

By using the Nearest Neighbor and the Maximum Value methods as well as the improved Adaptive Barnes interpolation algorithm, the data of Z9280 in Chengdu, Z9816 in Mianyang, and Z9817 in Nanchong at 9:20 am on July 2, 2018 were tested respectively, and the CAPPI images of several radars at a height of 3 km are fused as shown in Fig. 6.

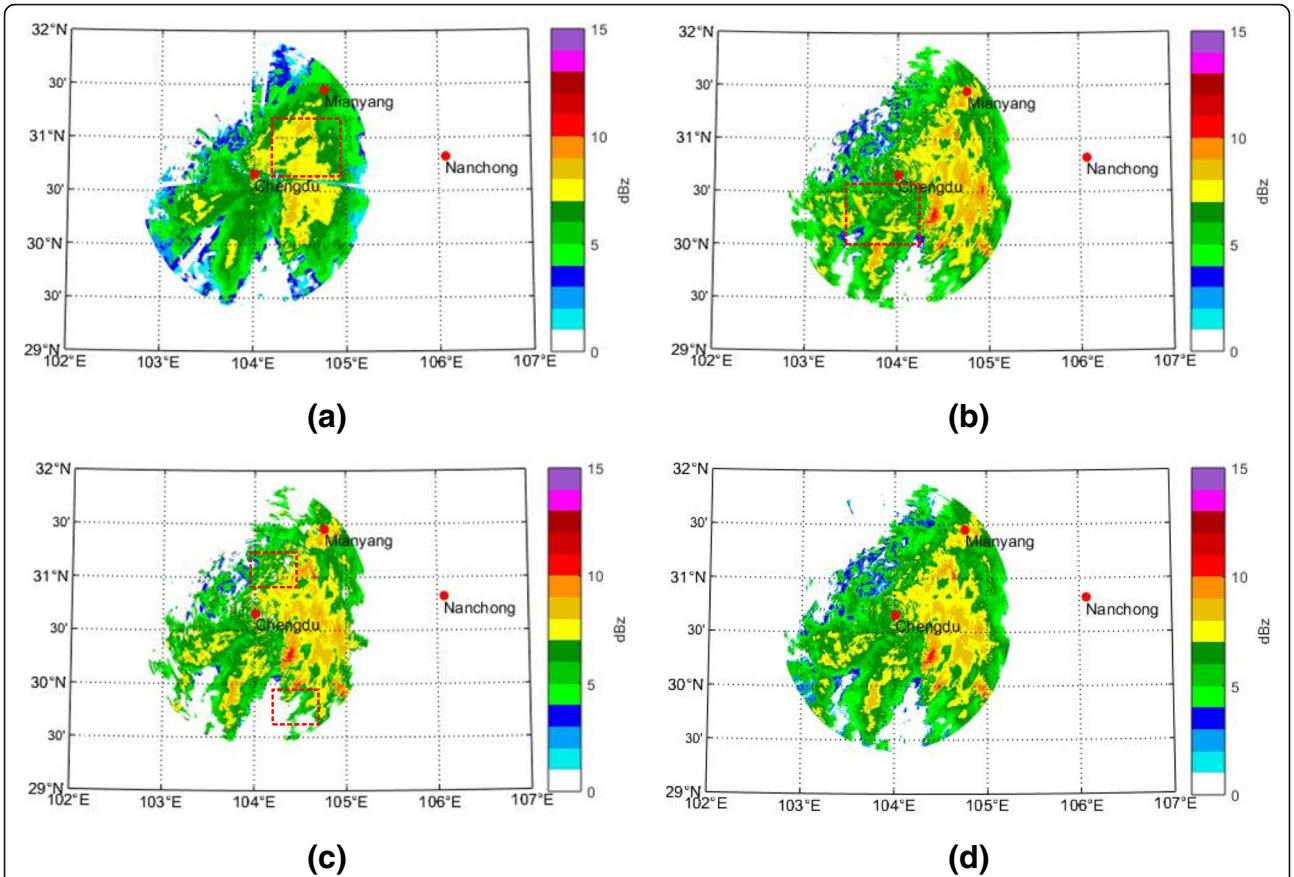

Fig. 5 CAPPI distribution map at 3 km altitude. **a** VHI, **b** the Nearest Neighbor, **c** 8-point Linear interpolation, and **d** the improved Adaptive Barnes interpolation

From Fig. 6c, it can be seen that the CAPPI map of reflectivity data is defective in some radial of radar Station in Nanchong as there are occlusions on these radial propagation paths, which prevents the area behind occlusions from being detected. Although the data of some radars is missing completely in some radial directions as a result of the conditional constraints, data of the commonly covered areas proved to be good, eliminating the problematic data by fusing multiple radar data. It turns out to be better if improved Adaptive Barnes interpolation method was used. The CAPPI image is smooth and continuous without obvious mutation.

In the Nearest Neighbor method, the closest data of the radar in the commonly covered areas of the radar is selected to fill the grid cell, leading to discontinuity and mutation. For instance, the Mianyang radar station has obvious sections and blanks from 50 to 90 km in the East as shown in Fig. 6d. The Maximum Value method fills the common detection areas with the maximum values of three radars in each grid unit. It can be seen that the data of the commonly covered areas increases generally. The decrease of detection accuracy caused by the increase of detection distance as shown in Fig. 6e is negligible. The Exponential Weighting method makes the weight of the close-range grid data larger, and the weight of the grid data far away from the radar is smaller. After combining the exponential weights of the grid with grid data, the mosaic images are effectively fused, and the position and intensity of strong precipitation are consistent with the single radar CAPPI image. In a single radar scan area, the mosaic after filtering

Table 3 The comparison results of interpolation methods

Category	VHI	Nearest Neighbor	8-point Linear	Adaptive Barnes
Proportion of points with valid data	59.32%	56.63%	55.07%	60.02%
Smoothness	Ordinary	Ordinary	Ordinary	Excellent
Continuity	Poor	Poor(mutation)	Excellent	Excellent
Heavy precipitation areas	disappeared	Accurate	Accurate	Accurate

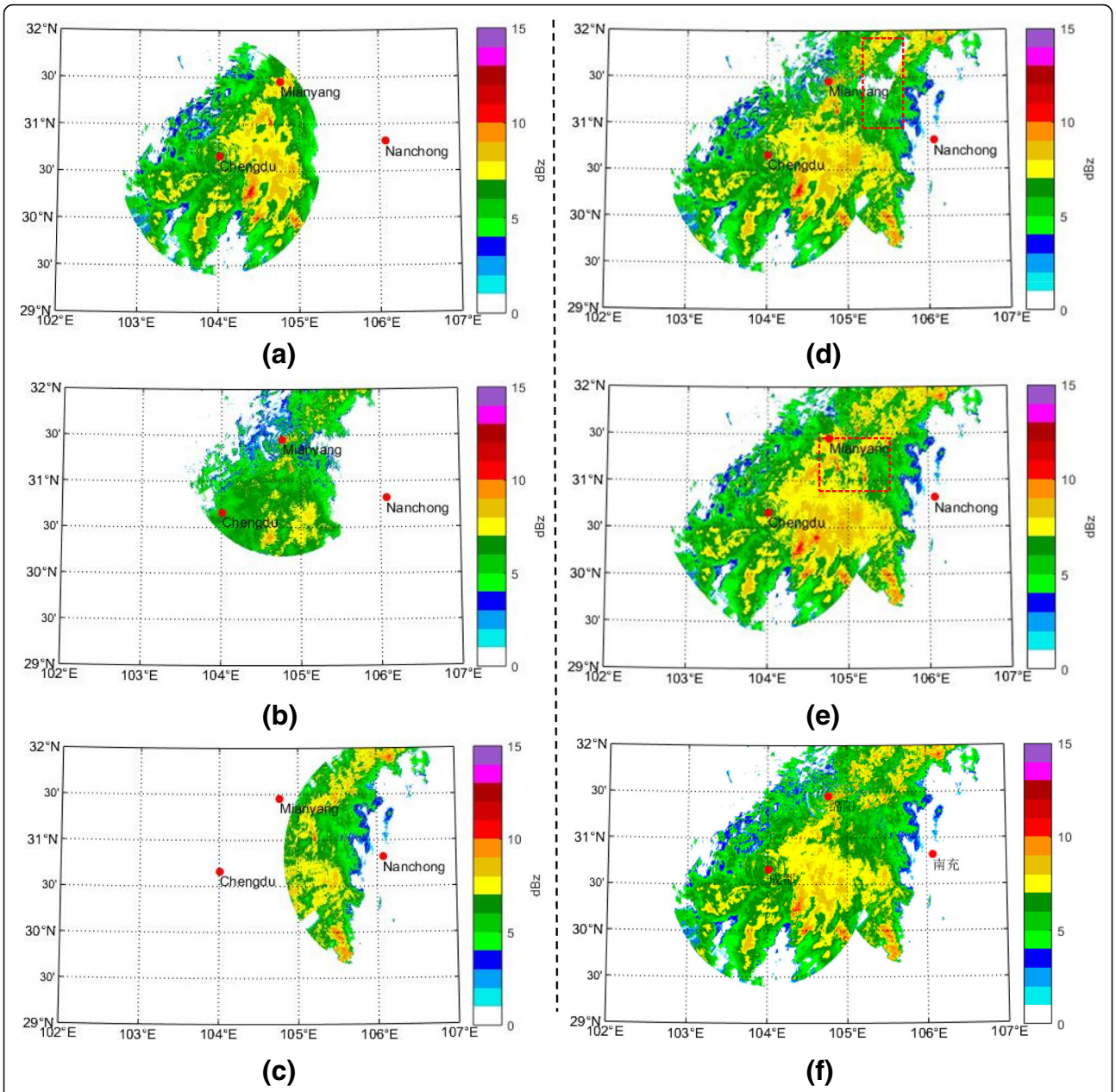

Fig. 6 Reflectivity mosaics of precipitation data at 3 km altitudes. **a**–**c** Are CAPPI map of Chengdu, Mianyang, Nanchong by the improved Adaptive Barnes interpolation algorithm. **d**–**f** The CAPPI mosaics with the Nearest Neighbor method, the Maximum method, and the Exponential Weighting method

Table 4 The comparison results of mosaics methods

Category		Nearest Neighbor	Maximum Value	Exponential Weighting
Continuity		Poor (missing massively)	Excellent	Excellent
Stability		Poor	Poor	Excellent
Heavy precipitation areas	Intensity	Greater	Standard	Standard
	Range	Larger	Standard	Standard

does not have excessive smoothness and blurred edges. And individual abnormal data is eliminated. The joint detection of multiple radars counteracts the problems of insufficient detection range, inadequate detection accuracy of single radar, and data quality affected by larger detection distance and occlusion. For example, there is a strip section in the west of Nanchong radar in Fig. 6c, smoothed continuously after the mosaic. Table 4 summarizes the performance of those mosaic methods from the continuity and stability of mosaics, and the intensity and range of heavy precipitation areas.

In order to compare the effect differences of these mosaics methods, a point A is obtained by projecting the center point of the triangle formed by the three radars onto the 3 km CAPPI plane, then three lines are constructed which are L1, L2 and L3, as shown in Fig. 7. The reflectivity values on the grid points on line L1, line L2 and line L3 are plotted in Fig. 8. As can be seen from Fig. 8, the general trend of reflectivity change along the lines after mosaicking with these methods are roughly the same. However, we can see that the amount of fluctuation is largest with the Nearest neighbor method in detail and the mean value is largest with the maximum value method. From Fig. 8b, it can be seen that there is a big error between the Maximum value method and others within 10 km from Mianyang radar station. In Fig. 8c, the first 30 km on the path is not in the common coverage area so that the line charts are overlapped. In general, the Index weight function has a stable and reliable performance.

In conclusion, the mosaic result of the Exponential Weighting has obvious advantages compared with other methods. It can also be applied to the high-precision three-dimensional mosaic of the national radars and improves the precision of weather forecast.

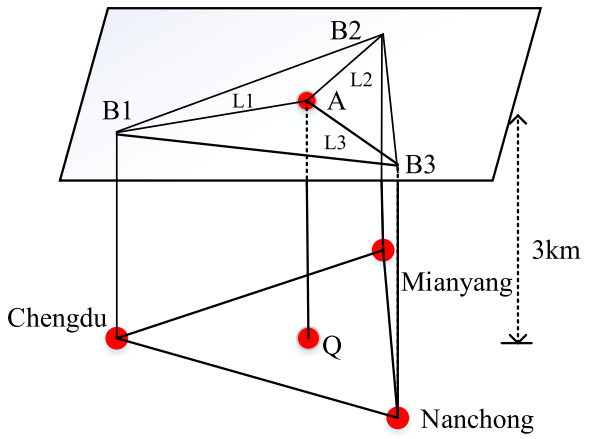

Fig. 7 An illustration of three verification paths

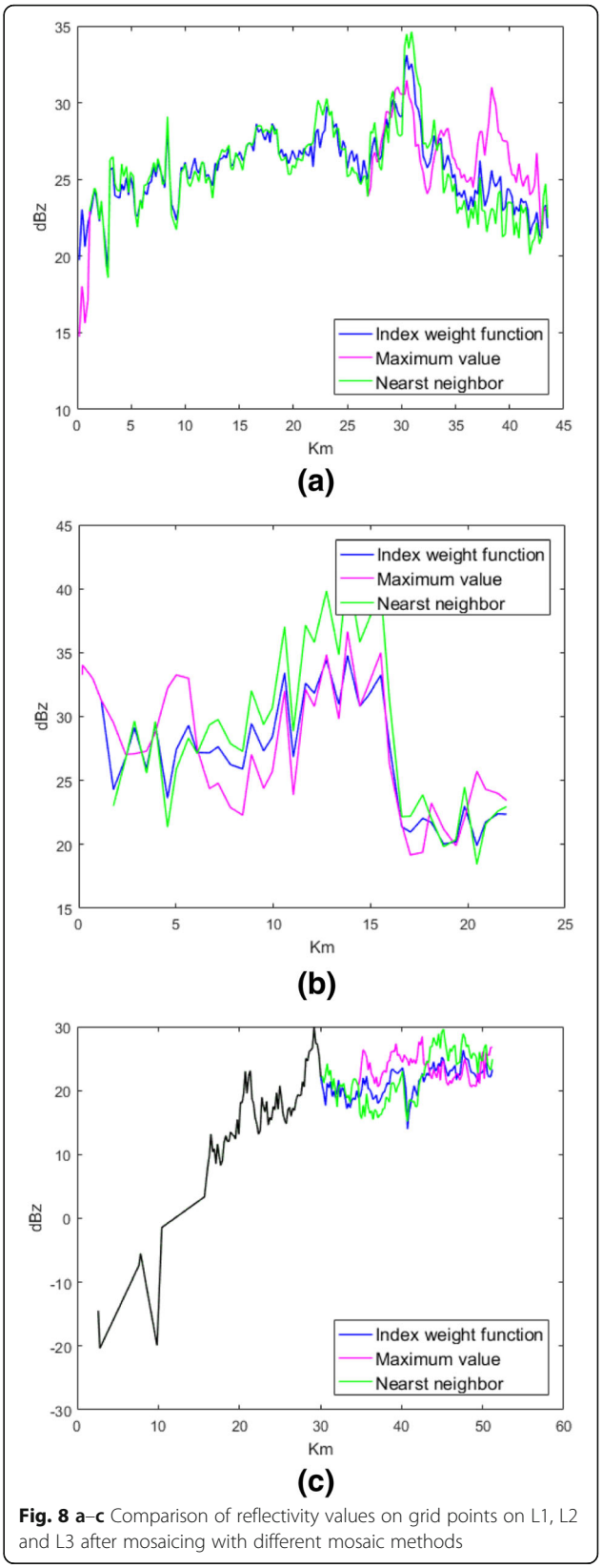

Fig. 8 a–c Comparison of reflectivity values on grid points on L1, L2 and L3 after mosaicing with different mosaic methods

6 Conclusions

In this paper, several interpolation and mosaic approaches are evaluated by using the raw data derived from the NEXRAD located in Chengdu, Mianyang, and Nanchong of Sichuan province in China. The Adaptive Barnes interpolation method is improved, making the smoothing parameters change flexibly with the spatial structure of radar data, while fully retaining the characteristics of the raw data. By comparing the CAPPI of reflectivity with the traditional inversion algorithm, the improved Adaptive Barnes interpolation method has obvious advantages in smoothness, continuity, and other precipitation characteristics. Besides, it makes up the sudden changing and empty data cell problems of the Maximum value method and the Nearest Neighbor method. The Mean deviation method can filter the error data caused by the poor quality radar data effectively and makes the data involved in multi-radars mosaic more credible. By conducting a large number of case experiments, it is found that the Exponential Weighting method can fuse the grid data of multiple radars effectually, and it can form continuous three-dimensional reflectivity analysis field.

The interpolation and three-dimensional mosaic of three Doppler weather radar data are realized. A new scheme of smooth parameter is proposed to keep good characteristics of the raw volume data. These methods can also be applied to the data interpolation of regional multi-radar or even to the high-precision three-dimensional mosaic of the national radars, and they can provide high spatial and temporal resolution three-dimensional grid data for the depth application of the NEXRAD.

Abbreviations

CAPPI: Constant altitude plan position indication; NEXRAD: The next generation weather radar; VHI: Vertical horizontal linear interpolation

Funding

This research was funded by the National Natural Science Foundation of China (award number U1733103), the Department of Science and Technology of Sichuan Province (award number 2016JY0106), and the Education Department of Sichuan Province (award number 16ZA0209), and College of Electronic Engineering of CUIT(the 2018 Innovation and Entrepreneurship Project).

Availability of data and materials

Data sharing not applicable to this article as no datasets were generated or analyzed during the current study.

Authors' contributions

MS proposed the study and wrote the manuscript, HW and conducted the experiments, ZL analyzed the data, MG revised the manuscript, ZX advised on the study design, and JL advised on the manuscript structure. All authors read and approved the final manuscript.

Competing interests

The authors declare that they have no competing interests.

Publisher's Note

Author details

[1]College of Electronic Engineering, Chengdu University of Information Technology, Chengdu 610225, Sichuan, China. [2]Foshan Tornado Research Center, Foshan Meteorological Service, Foshan 528000, China. [3]The Second Research Institute of CAAC, Chengdu 610041, Sichuan, China.

Received: 27 February 2019 Accepted: 3 May 2019
Published online: 03 June 2019

References

1. Z. Yuanyuan, Y. Xiaoding, et al., Analysis of a strong classic supercell storm with Doppler weather radar data[J]. Acta Meteor Sin **62**(3), 317–328 (2004)
2. R.J. Serafin, J.W. Wilson, Operational weather radar in the United States: progress and opportunity[J]. Bull. Am. Meteorol. Soc. **81**(3), 501–518 (2008)
3. J. Zhang, K. Howard, C. Langston, Three- and four-dimensional high-resolution National Radar Mosaic[J]. Proc Erad, 105–108 (2004)
4. C. Langston, J. Zhang, K. Howard, Four-dimensional dynamic radar mosaic[J]. J Atmospheric Oceanic Technol **24**(5), 776–790 (2007)
5. M.A. Askelson, J.P. Aubagnac, S.J.M. An, Adaptation of the Barnes filter applied to the objective analysis of radar data[J]. Mon. Weather Rev. **128**(9), 3050–3082 (2010)
6. V. Lakshmanan, T. Smith, K. Hondl, et al., A real-time, three-dimensional, rapidly updating, heterogeneous radar merger technique for reflectivity, velocity, and derived products[J]. Weather Forecast. **21**(5), 802–823 (2006)
7. J. Zhang, K. Howard, J.J. Gourley, Constructing three-dimensional multiple-radar reflectivity mosaics: examples of convective storms and Stratiform rain echoes[J]. J Atmos Oceanic Technol **22**(1), 30–42 (2005)
8. D.P. Jorgensen, P.H. Hildebrand, C.L. Frush, Feasibility test of an airborne pulse-Doppler meteorological radar[J]. J. Appl. Meteorol. **22**(5), 744–757 (1972)
9. L. Jay Miller, C.G. Mohr, A.J. Weinheimer, The simple rectification to Cartesian space of folded radial velocities from Doppler radar sampling[J]. J Atmos Oceanic Technol **3**(1), 162–174 (2013)
10. C.G. Mohr, R.L. Vaughan, An economical procedure for Cartesian interpolation and display of reflectivity factor data in three-dimensional space[J]. J. Appl. Meteorol. **18**(5), 661–670 (1979)
11. S.S. Weygandt, A. Shapiro, K.K. Droegemeier, Retrieval of model initial fields from single-Doppler observations of a supercell thunderstorm. Part I: Single-Doppler velocity retrieval[J]. Mon. Weather Rev. **130**(130), 433 (2002)
12. A. Shapiro, P. Robinson, J. Wurman, J. Gao, Single-Doppler velocity retrieval with rapid-scan radar data[J]. J Atmos Oceanic Technol **20**(12), 1758–1775 (1925)
13. P.M. Pauley, X. Wu, The theoretical, discrete, and actual response of the Barnes objective analysis scheme for one- and two-dimensional fields[J]. Mon. Weather Rev. **118**(5), 1145–1164 (1990)
14. R.J. Trapp, C.A.I. Doswell, Radar data objective analysis[J]. J Atmos Oceanic Technol **17**(2), 105–120 (2000)
15. Y.X. Huang, Y. Zhang, Comparison of interpolation schemes for the Doppler weather radar data[J]. Remote Sens Inf **21**(2), 39–45 (2008)
16. S.L. Barnes, A technique for maximizing details in numerical weather map analysis[J]. J. Appl. Meteorol. **3**(4), 396–409 (1964)
17. J. Liu, Primary study on three-dimensional gridding weather radar data and CINRAD mosaic[J]. J Anhui Agric Sci (2010)
18. Y.J. Xiao, L. Liu, Study of methods for interpolating data from weather radar network to 3-D grid and mosaics[J]. Acta Meteor Sin **64**(5), 647–656 (2006)
19. Li Y. Study of method for new generation weather radar mosaic based on GIS[D]. School of information and software engineering
20. G.M. Heymsfield, Statistical objective analysis of dual-Doppler radar data from a tornadic storm[J]. J. Appl. Meteorol. **15**(15), 59–68 (2010)
21. Y.H. Lee, S.A. Kassam, Generalized median filtering and related nonlinear filtering techniques[J]. Acoust Speech Signal Process IEEE Trans **33**(3), 672–683 (1985)
22. J. Wurman, S. Heckman, D. Boccippio, A bistatic multiple-Doppler radar network[J]. J. Appl. Meteorol. **32**(12), 1802–1814 (1993)
23. P.S. Ray, K.K. Wagner, K.W. Johnson, et al., Triple-Doppler observations of a convective storm[J]. J. Appl. Meteorol. **17**(8), 1201–1212 (1978)
24. C.A. Doswell, Obtaining meteorologically significant surface divergence fields through the filtering property of objective analysis[J]. Mon. Weather Rev. **105**(7), 885–892 (1977)